Title

Increased nanoparticle-loaded exogenous macrophage migration into the brain following PDT-induced blood–brain barrier disruption

Journal

Lasers in Surgery and Medicine, 45(8)

ISSN

0196-8092

Authors

Madsen, Steen J
Gach, H Michael
Hong, Seok Jin
et al.

Publication Date

2013-10-01

DOI

10.1002/lsm.22172

Peer reviewed

Published in final edited form as:
Lasers Surg Med. 2013 October ; 45(8): 524–532. doi:10.1002/lsm.22172.

Increased Nanoparticle-Loaded Exogenous Macrophage Migration Into the Brain Following PDT-Induced Blood–Brain Barrier Disruption

Steen J. Madsen, PhD[1,*], **H. Michael Gach, PhD**[2], **Seok Jin Hong, MD**[3], **Francisco A. Uzal, DVM**[4], **Qian Peng, PhD**[5], and **Henry Hirschberg, MD, PhD**[6]

[1]Department of Health Physics and Diagnostic Sciences, University of Nevada, Las Vegas, Nevada 89154

[2]Departments of Radiology and Bioengineering, University of Pittsburgh, Pittsburgh, Pennsylvania 15213

[3]Department of Otorhinolaryngology-Head and Neck Surgery, Sungkyunkwan University School of Medicine, Seoul, Korea

[4]School of Veterinary Medicine, University of California, Davis, San Bernardino, California

[5]Department of Pathology, Oslo University Hospital, Montebello 0310, Oslo, Norway

[6]Beckman Laser Institute and Medical Clinic, University of California, Irvine, California 92612

Abstract

Background and Objective—Photodynamic therapy (PDT)-induced disruption of the blood–brain barrier (BBB) has been investigated as a technique for the delivery of therapeutic agents to selective regions of the brain. The purpose of this study was to determine the effects of PDT on the migration of systemically administered exogenous macrophages (Ma) loaded with iron oxide nanoparticles in non-tumor bearing rats.

Materials and Methods—A control group consisting of three Sprague–Dawley rats was injected with iron oxide-loaded rat alveolar Ma via jugular vein catheter while two animals were subjected to intracranial injection of iron oxide-loaded Ma. PDT-treated animals were injected with photosensitizer ($AlPcS_{2a}$; 1 mg/kg i.p.) followed by light irradiation (wavelength = 670 nm; light dose = 2.5 J) 48 hours later. Light irradiation was performed through the skull. Prior to light irradiation, iron oxide-loaded Ma were administered to each animal. Animals in all groups were imaged in a 7 Tesla (T) magnetic resonance (MR) imager to determine the extent of PDT-induced edema and to evaluate for the presence of iron oxide nanoparticles. Animals were sacrificed 7 days post-Ma administration and their brains analyzed for the presence of iron oxide using Perls staining.

[*]Correspondence to: Steen J. Madsen, PhD, Department of Health Physics and Diagnostic Sciences, University of Nevada, Las Vegas, Box 453037, 4505 South Maryland Pkwy, Las Vegas, NV 89154. steen.madsen@unlv.edu.

Conflict of Interest Disclosures: All authors have completed and submitted the ICMJE Form for Disclosure of Potential Conflicts of Interest and none were reported.

Results—Significant uptake of iron oxide nanoparticles by rat alveolar Ma was observed thus providing the rationale for their use as delivery vectors. Histopathological analyses failed to find evidence of iron oxide in normal rat brain. Accumulations of iron oxide-loaded Ma were observed in both MR images and histological sections of non-tumor bearing rat brain following PDT-induced disruption of the BBB.

Conclusions—MR imaging was shown to be useful for localizing iron-oxide loaded Ma in rat brains. Exogenous Ma are incapable of traversing the normal BBB and therefore, the use of Ma as delivery vehicles into the brain requires selective disruption of the BBB.

Keywords

glioma; iron oxide nanoparticles; photodynamic therapy; magnetic resonance imaging

INTRODUCTION

Malignant gliomas are the most common primary brain tumors in adults. The most aggressive of these tumors, glioblastoma multiforme (GBM), is characterized by a number of histological features including significant proliferation, invasion, angiogenesis, and necrosis. Even with substantial improvements in conventional treatments consisting of surgery, radiation therapy, and chemotherapy, the prognosis for patients with this disease has not improved significantly over the past four decades: median survival is approximately 12–14 months [1].

One of several factors limiting the treatment efficacy for gliomas is the presence of the blood–brain barrier (BBB) which prevents many soluble materials, pathogens, and circulating cells from entering the brain. The BBB is formed by tightly connected brain capillary endothelial cells that prevent passage of most biological molecules. This impermeability prevents harmful substances in the blood plasma from entering the brain. Unfortunately, this protective barrier also prevents many effective anti-cancer agents from reaching infiltrating glioma cells that have migrated into normal brain from the solid tumor mass. Failure to eradicate these infiltrating cells following MRI-defined complete surgical resection of the main tumor mass invariably results in tumor recurrence in the resection margins [2]. Therefore, therapy directed toward sterilization of the resection margins are of interest.

The development of drugs capable of penetrating the BBB is an active area or research as it impacts not only cancer patients but also those with neurodegenerative diseases. Presently, temozolomide (TMZ) is the only clinically used chemotherapeutic agent capable of crossing the BBB and, although clinical trials have demonstrated some benefit, median survival of GBM patients (14.6 months) receiving this drug in combination with radiation therapy improved by only a few months over those receiving the standard-of-care treatment [3]. Therefore, other approaches directed toward sterilization of the resection margins are clearly of interest.

The ability of monocytes to migrate, accumulate and mature into macrophages (Ma) both within and at the periphery of tumors, provides the rationale for their use as delivery vectors

in both diagnostic and therapeutic oncologic applications [4–10]. In particular, Ma may be useful in therapeutic applications involving high-grade gliomas such as GBM since this tumor is characterized by large areas of hypoxia and necrosis due to its rapid proliferation. In this context, the utility of Ma as delivery vehicles is critically dependent on their ability to penetrate both relatively normal and leaky BBB and/or blood–tumor barrier (BTB) associated with the tumor and surrounding vasculature. Ma-based vectorization of genes, drugs, or nanoparticles is therefore of interest for cancer therapy in the brain as a way of bypassing the BBB [11,12]. We have recently reported the ability of photodynamic therapy (PDT), employing either exogenous or endogenous photosensitizers, to reversibly open the BBB in selected areas of the brain to drugs and MRI contrast [13–15]. Extending this concept, PDT should also be effective not only in increasing the permeability of the BBB to substances that normally do not penetrate into the brain, but also to viable Ma. Ma loaded with nanoparticles could therefore be used as delivery vectors to target specific sites in the brain where the BBB has been opened. Chemical opening of the BBB has been shown to increase the migration of fluorescent labeled monocytes into normal brain in mice [16]. This method, although interesting, is limited by a lack of site specificity necessary for postoperative treatment. The ability to increase loaded Ma migration and concentration into targeted areas in the brain, such as the postoperative resection margin by PDT, is therefore of significant clinical relevance. This concept is illustrated in Figure 1.

In the study reported here, we have investigated the effects of PDT on the migration of i.v. injected exogenous Ma loaded with iron oxide nanoparticles in non-tumor bearing rats. We have limited PDT treatment to normal brain in order to mimic the environment following surgical resection of bulk tumor, where glioma cells have migrated into normal brain adjacent to the tumor site. The iron oxide nanoparticles are MR contrast agents and, as such, they were used in conjunction with MR imaging to evaluate the extent of loaded Ma infiltration in rat brain.

MATERIALS AND METHODS

Cell Lines

Rat alveolar Ma (NR8383; ATCC# CRL-2192) were obtained from the American Type Culture Collection (Manassas, VA). Ma were maintained in Dulbecco's modified Eagle medium (DMEM) with high glucose (Invitrogen Corp., Carlsbad, CA) supplemented with 10% fetal bovine serum (FBS), 25 mM HEPES buffer (pH 7.4), penicillin (100 U/ml), and streptomycin (100 μg/ml) at 37°C and 5% CO_2.

Experimental Animals

Inbred male Sprague–Dawley rats (Charles River, Wilmington, MA) weighing approximately 350 g were used in this study. Animal care and protocols were in accordance with institutional guidelines. Animal holding rooms were maintained at constant temperature and humidity on a 12-hour light and dark schedule at an air exchange rate of 18 per hour.

Nanoparticles

The superparamagnetic iron oxide contrast agent, Feridex I.V.® (Advanced Magnetics, Inc., Cambridge, MA) was used in the *in vivo* migration studies since they are easily identified in MR images and histological sections. Their core consists of iron crystals incompletely coated with Dextran T-10 and have a hydrodynamic size of 120–180nm (mean particle size of 58.5 nm).

Photosensitizer

Aluminum phthalocyanine disulfonate ($AlPcS_{2a}$: Frontier Scientific, Inc., Logan, UT) is a second-generation photosensitizer characterized by its high absorption efficiency in the far red (670–675 nm) part of the visible spectrum. Due to its amphiphilicity, $AlPcS_{2a}$ localizes to the plasma membrane which makes it ideally suited for photochemical internalization applications [17].

Nanoparticle Uptake

NR8383 rat alveolar Ma were seeded in 35 mm cell culture dishes at 10^6 Ma in 2 ml of culture medium. The dishes were incubated overnight to allow the cells to settle and adhere to the plastic. Culture medium was exchanged for 100 μl of iron oxide in 1.9 ml of culture medium (200 μg Fe/ml). The Ma and iron oxide were incubated together for 24 hours at 37°C and rinsed three times with Hanks' Balanced Salt Solution with calcium chloride and magnesium chloride (HBSS, Gibco, Carlsbad, CA) to wash away the excess non-ingested iron oxide. Iron oxide-loaded Ma were then detached with trypsin, washed, and counted.

Iron uptake was quantified using inductively coupled plasma atomic emission spectrometry (ICP-AES). Briefly, Iron oxide-loaded Ma were transferred into 15 ml centrifuge tubes and centrifuged at 600 rpm for 7 minutes. The resultant cell pellet was washed twice with phosphate buffered saline (PBS) in order to remove any loose particles. The pellet was transferred to an epitube and mineralized in a heat block adjusted to 80°C with 70% HNO_3 for 1.5 hours. Twenty microliters of 30% H_2O_2 was added and mineralization was resumed for an additional 3.5 hours. Samples were then diluted with deionized water to obtain a HNO_3 concentration of 5% in a final volume of 10 ml, then filtered using a 0.45-μm membrane and stored at 4°C until ICP-AES analysis. Samples were measured using an iCAP 6500 series (Thermo Scientific, Inc., Cambridge, UK) ICP-AES at a wavelength of 238.2 nm. Calibration was performed with iron standards prepared from SPEX CertiPrep Iron Standard (CAT# CLFE 2-2Y: Fisher Scientific, Inc., Pittsburgh, PA). The amount of iron (pg) was calculated from the iron concentration (ppm) detected by the instrument according to:

$$\mathrm{Fe\,(pg)} = \mathrm{measured\,Fe\,(mg/ml)} \times \mathrm{sample\,volume\,(ml)} \times 10^9\,\mathrm{pg/ml}$$

Intracellular iron content (pg/cell) was determined simply by dividing the amount of iron by the number of cells in each run.

Iron Oxide-Loaded Ma Administration in Control Animals

Three rats were subjected to i.v. administration of 4.5×10^5 nanoparticle-loaded Ma via indwelling jugular catheters. Two additional animals were subjected to direct intracranial injection of 20,000 rat alveolar Ma in 10 μl PBS. Ma were incubated with iron oxide as previously described. Intracranial injection was accomplished using a stereotactic frame (David Kopf Instruments, Tujunga, CA). Anesthetized rats (gas inhalation: 3% isoflurane in oxygen) were fixed in the stereotactic frame and their skin incised. A 1.0-mm burr hole was made at the following coordinates: 1 mm posterior to the bregma, 2 mm to the right of the midline, and at a depth of 2 mm. The injection device consisted of a 30-G blunt cannula connected through a catheter (Hamilton Co., Reno, NV) to an infusion pump (Harvard Apparatus, Holliston, MA). The cannula was fixed in the electrode holder of the stereotactic frame, and then vertically introduced into the brain. Following the 2 minures injection period, the cannula remained in place for an additional 2 minutes after which the burr hole was closed with bone wax and the skin sutured.

PDT-Induced BBB Disruption in Non-Tumor Bearing Rats

For the surgical procedures, animals were anesthetized via gas inhalation as previously described. Buprenophine (0.05 mg/kg i.p.) was used as a postoperative analgesic and was administered immediately following surgery and twice per day for 2 days thereafter. All animals were euthanized at the conclusion of the study, or at the first sign of distress. Euthanasia was accomplished via CO_2 inhalation followed by brain extraction.

Animals (n = 5) were injected with photosensitizer ($AlPcS_{2a}$; 1 mg/kg i.p.) followed by light irradiation 48 hours later. Immediately prior to light irradiation, 2.5×10^5 iron oxide-loaded rat Ma (in 0.5 ml PBS) were administered to each animal via an indwelling jugular vein catheter. The Ma were incubated with iron oxide as previously described. Light irradiation was accomplished by immobilizing anesthetized animals in the stereotactic frame. A skin incision was made exposing the skull and an optical fiber coupled to a 670 nm diode laser (Intense, New Brunswick, NJ) was placed in contact with the surface of the skull 1 mm posterior to the bregma and 2 mm to the right of the midline. The optical fiber (600 μm core diameter) was terminated with a microlens resulting in a high degree of beam uniformity (±15%). Animals were exposed to 10 mW laser light for 250 seconds (total light dose of 2.5 J). Following PDT, the wound was closed with sutures and the animals were placed in a recovery cage.

Magnetic Resonance Imaging

Isoflurane anesthetized animals were imaged on days 1, 3, and 7 post-PDT in a 7-T small bore animal MR scanner (Bruker Corp., Billerica, MA). A small surface coil was placed on top of the target area and T_2^*-weighted multiple gradient echo (MGE) pulse sequences (TE = 4 milliseconds +n ×3.63 milliseconds, n = 0–14; TR = 1.9 seconds; flip angle = 90°) were used to evaluate for the presence of iron oxide-loaded Ma. Superparamagnetic contrast agents such as Feridex cause significant shortening of T_2^* relaxation times with concomitant loss of signal in the targeted tissue. T_2-weighted spin echo pulse sequences (TR/TE = 4,200 milliseconds/36 milliseconds) were used to determine the extent of edema caused by PDT-

induced BBB disruption. Other major MR imaging parameters were: matrix size = 128 ×128, field-of-view = 3.5 cm ×3.5 cm, 1 mm slice thickness and number of acquisitions (NA) = 1.

Histological Preparation

Animals in the PDT study were euthanized 7 days post-PDT and their brains extracted. Brains were fixed by immersion in 10% buffered (pH 7.2) formalin prior to paraffin embedding. Coronal sections (4-μm thick) were obtained at locations near the light source. Iron-loaded Ma were detected using Perls Prussian Blue staining. Slices were incubated with 2% potassium ferrocyanide (Perls reagent, Sigma, St. Louis, MO) in 2% HCl, washed and counterstained with erythrosine. Animals in the non-treated control groups were sacrificed 7 days post-Ma administration, their brains extracted, fixed, paraffin embedded, sectioned, and stained with Perls and hematoxylin and eosin (H&E).

RESULTS

Uptake of Iron Oxide Nanoparticles

As illustrated in Figure 2, iron oxide uptake in rat Ma was approximately linear over the concentration range investigated (0–400 μg/ml). Higher concentrations were not attempted since some toxicity was observed at 400 μg/ ml. Based on these data, a concentration of 200 μg/ml was used in subsequent studies.

Iron Oxide-Loaded Macrophage Administration in Control Animals

Histological sections of normal rat brain showed no evidence of iron oxide following i.v. administration of 4.5×10^5 nanoparticle-loaded Ma (Fig. 4a). The lack of iron oxide was also verified on T_2^*-weighted MR images which appeared normal (data not shown). In contrast, iron oxide was clearly visible in MR images (Fig. 3a and b) and histological sections (Fig. 3c and d) following direct intracranial injection of iron oxide-loaded Ma. The area of the signal voids in the T_2^*-weighted images were approximately 100–300 times larger than the corresponding Perls blue stained regions in the histology slides. For example, the signal void diameters typically ranged between 1 and 2 mm compared to approximately 0.1 mm for the Perls blue stained regions. This discrepancy is caused by the extent of the magnetic susceptibility gradiant created by the paramagnetic iron oxide nanoparticles.

PDT-Induced BBB Disruption and Macrophage Migration

The presence of iron oxide in non-tumor bearing rats subjected to PDT is indicated by the Perls stain (blue) around the periphery of the PDT-affected region (Fig. 4b). Higher magnification images (Fig. 4c) show a combination of resident brain cells as well as endogenous and exogenous iron oxide-loaded Ma that have infiltrated the PDT-treated region. In several sections, loaded Ma could be seen clustered around capillary vessels (Fig. 4d) illustrating their migration out of the vasculature. No loaded Ma could be found in other areas of the brain remote from the irradiated site in either cerebral hemisphere.

The hyperintense regions in the T_2-weighted MR images (Fig. 5a and b) correspond to edema due to PDT-induced disruption of the BBB. Of particular interest are the T_2^* images

(Fig. 5c and d) which show a number of large signal voids lining the periphery of the PDT-treated region. Since the locations of the voids and blue Perls stain (Fig. 4b) are similar, it is highly likely that the signal voids are caused by the presence of iron oxide-loaded Ma.

DISCUSSION

The primary treatment for high-grade gliomas such as GBM is surgical resection. This is typically followed by secondary treatments consisting of radiation and chemotherapy that aim to eradicate infiltrating cells in the resection margin and normal brain. As evidenced by high recurrence rates, standard GBM treatment regimens are rather ineffective suggesting the need for improved local therapies such as the Ma-based delivery approach described herein. The primary objective of the proposed treatment approach is to eradicate clusters of infiltrating glioma cells in normal brain, that is, tumor cells protected by the normal BBB. It is precisely for this reason that tumor-bearing animals were not used in any of the studies.

The results presented in Figure 2 show that rat alveolar Ma are readily capable of ingesting iron oxide nano-particles. This is in good agreement with the results of other investigators who have used iron oxide labeled monocytes/Ma as magnetic resonance imaging contrast agents [18–20].

The absence of iron oxide nanoparticles in normal rat brain suggests that exogenous Ma are incapable of penetrating normal BBB. The findings in normal brain are hardly surprising since few substances are capable of crossing the intact BBB. This is due to the architecture of the barrier which is formed by tightly connected brain capillary endothelial cells that seal the paracellular spaces and form a continuous physical barrier between the CNS and blood circulation [21]. Consequently, almost all large-molecule pharmaceuticals (peptides, recombinant proteins, monoclonal antibodies, and gene therapeutics) and 98% of small molecules are incapable of penetrating the BBB [22]. The few drugs capable of crossing the BBB have a number of characteristics in common including small size (<400 Da), high lipid solubility and passage across the barrier by passive diffusion.

The present studies were limited to normal brain in order to mimic the environment following surgical resection of bulk tumor. The primary challenge for the successful treatment of high-grade gliomas, such as GBM, is the eradication of infiltrating tumor cells in normal brain which are protected by the patent BBB. In contrast, the delivery of drugs to the tumor mass is less challenging due to the leaky BTB. For example, Valable et al. [20] have observed evidence of iron oxide particles in rat gliomas following intravenous administration of iron oxide-loaded murine Ma.

Iron oxide nanoparticles (Feridex) were used in these studies since they can be visualized in MR images and, hence, they can be used as noninvasive markers to track Ma migration. These superparamagnetic contrast agents significantly alter the local magnetic field resulting in susceptibility artifacts at their point of localization which has the effect of enhancing T_2 relaxation resulting in a strong decrease in signal intensity [23]. Iron oxide is readily taken up by Ma, especially Kupffer cells in the liver thus providing the rationale for their use as contrast agents for the detection of focal liver lesions [24]. Not surprisingly, rat alveolar Ma

(Fig. 2) also show significant uptake of iron oxide nanoparticles and the susceptibility effects caused by these contrast agents in normal rat brain are readily apparent in Figure 3a and b. Although Feridex is no longer available for clinical use, there are a number of other iron oxide-based contrast agents (e.g., ferumoxytol) that appear to be suitable candidates for tracking Ma migration via MR imaging [25]. The poor cellular uptake of ferumoxytol is unlikely to be an issue since the contrast agent is not administered directly, but rather, via Ma which are preloaded with nanoparticles *in vitro* prior to systemic administration. Although the rate of nanoparticle ingestion is somewhat dependent on the particle type, the desired concentration can be achieved simply by varying the incubation conditions (e.g., nanoparticle concentration and incubation time).

The data presented in Figure 4b show significant iron oxide accumulation when Ma administration is preceded by PDT. This is almost certainly due to PDT-induced disruption of the BBB facilitating Ma entry into the brain. Further evidence of this is presented in Figure 4d which shows clustering of iron-oxide loaded Ma around brain capillaries. These Ma have penetrated the leaky capillaries just prior to sacrifice and therefore have not had time to migrate from their source. The T_2^*-weighted MR images (Fig. 5c and d) provide additional verification of iron oxide accumulation in the form of multiple signal voids lining the border of the PDT-affected region. The extensive edema evident in the T_2-weighted images (Fig. 5a and b) suggest extensive PDT-induced disruption of the BBB.

Based on the histologic sections and the MR images, Ma infiltration appears to be limited to the periphery of the PDT-treated region. This is likely due to the high fluence rates near the fiber resulting in a collapse of the vascular supply. Based on the fiber diameter (600 μm) and the incident power (10 mW), the surface irradiance was approximately 3.5 W/cm^2. Such high irradiance PDT is certainly capable of causing vascular damage as confirmed by the presence of high levels of edema in Figure 5a and b. This is unlikely to be an issue in the clinical setting since the irradiation geometry will be different and the bulk of the tumor mass has been surgically resected. Instead of using surface irradiation, it is envisioned that PDT would be performed via insertion of an optical fiber into an indwelling balloon applicator placed into the resection cavity of the patient [26]. The balloon applicator stabilizes the resection cavity and provides uniform light dosimetry throughout the margins.

In the present work, the intracranial light distribution was difficult to estimate since *in situ* measurements were not performed. Due to the thinness of the rat skull (a few 100 μm) and its transparency to 670 nm light, it is estimated that at least 90% of the light energy passed through the skull. However, due to strong backscatter, the light dose near the surface of the brain will be many times higher than the incident exposure [27]. The penetration depth of 670 nm light in normal rat brain is approximately 1–3 mm [28]. This is in qualitative agreement with previous studies showing PDT-induced BBB disruption to depths approaching 5 mm using an identical surface irradiation geometry [14].

Site-specific disruption of the BBB has been accomplished by a number of techniques including focused ultrasound (FUS) and PDT [29]. The feasibility of MR image-guided FUS for the delivery of antibodies, chemo-therapeutics, and nanoparticles has been demonstrated in a number of rodent models [30–33]. Collectively, these studies show that BBB opening

occurs over a relatively short time span ranging from a few minutes to 6 hours following sonication [34] which may be sufficient for many neurologic applications but may be inadequate to maintain the high titers of chemotherapeutic agents necessary for the treatment of gliomas, thus providing the rationale for PDT-induced BBB disruption. In a recent study, the effects of PDT on the BBB in rats were studied using contrast-enhanced MRI [13]. The data showed that localized reversible disruption of the BBB is sensitively dependent on both light fluence and fluence rate. Incident light powers exceeding 10 mW induced substantial BBB disruption as evidenced from pronounced brain edema which resulted in significant morbidity and, in some cases, death. Below this light threshold, BBB disruption was found to be temporary in nature, opening rapidly following treatment, and approximately 90% restored 72 hours later. This time interval affords an opportunity for localized delivery of substances, for example, loaded Ma, that otherwise would be excluded from the brain due to their inability to penetrate the BBB.

The mechanisms of PDT-induced BBB opening are not known but likely include direct PDT effects on the endothelial cytoskeleton resulting in cell rounding and contraction, which may be due to PDT-induced microtubule depolymerization [35]. Additionally, both the formation and enlargement of endothelial gaps have been observed in response to PDT [36].

From a clinical perspective, the use of Ma as delivery vehicles could be accomplished in a relatively straightforward manner, for example, by isolating monocytes from a patient (which differentiate into Ma *ex vivo*), loading them with gold nanospheres (AuNS) and then re-injecting them into the patient. The ability of AuNS to convert near infrared light (NIR) to heat far exceeds that of conventional dyes and therefore they have the potential to be used in hyperthermia applications such as photothermal therapy (PTT). The goal of PTT in this context would be to induce rapid heating in tumors infiltrated with AuNS-loaded Ma, while minimizing thermal diffusion to surrounding normal tissue. For example, in a previous *in vitro* study, NIR laser-irradiated multicell human glioma spheroids, infiltrated with AuNS-loaded murine monocytes, demonstrated complete growth inhibition in an irradiance dependent manner [37].

In addition to thermal-based therapies, Ma may also be useful in PDT applications where they can act as delivery vehicles for nanoparticle–photosensitizer constructs. Examples include the incorporation of photosensitizers into modified silica nanoparticles with antibody targeting, the incorporation of photosensitizers into lipoprotein nano-particles and the use of nanoparticle–photosensitizer conjugates where the nanoparticle serves as the primary light absorber and then activates the photosensitizer via FRET [38].

In the case of gliomas, the use of autologous Ma offers several advantages. As shown in this work, systemically administered Ma could be made to selectively accumulate in site-specific regions where the BBB has been disrupted (such as the resection cavity). Additionally, their *ex vivo* preparation and subsequent reinjection into patients is far simpler in comparison to other techniques involving non-circulating cells such as stem cells.

Acknowledgments

The authors are grateful for support from the Norwegian Radium Hospital Research Foundation. Portions of this work were made possible through access to the LAMMP Program NIBIB P41EB015890 and the Chao Cancer Center Optical Biology Shared Resource at UCI. Steen Madsen was supported, in part, by the Tony and Renee Marlon Charitable Foundation.

References

1. Holdhoff M, Grossman SA. Controversies in the adjuvant therapy of high-grade gliomas. Oncologist. 2011; 16:351–358. [PubMed: 21339260]
2. Petrecca K, Guiot M-C, Panet-Raymond V, Souhami L. Failure pattern following complete resection plus radiotherapy and temozolomide is at the resection margin in patients with glioblastoma. J Neurooncol. 2013; 111:19–23. [PubMed: 23054563]
3. Sathornsumetee S, Rich JN. Designer therapies for glioblastoma multiforme. Ann NY Acad Sci. 2008; 42:108–132. [PubMed: 18990124]
4. Knowles HJ, Harris AL. Macrophages and the hypoxic tumour microenvironment. Front Biosci. 2007; 12:4298–4314. [PubMed: 17485376]
5. Murdoch C, Lewis CE. Macrophage migration and gene expression in response to tumor hypoxia. Int J Cancer. 2005; 117:701–708. [PubMed: 16106399]
6. Fleige G, Nolte C, Synowitz M, Seeberger F, Kettenmann H, Zimmer C. Magnetic labeling of activated microglia in experimental gliomas. Neoplasia. 2001; 3:489–499. [PubMed: 11774031]
7. Jackson H, Muhammad O, Daneshvar H, Nelms J, Popescu A, Vogelbaum MA, Burchez M, Toms SA. Quantum dots are phagocytized by macrophages and colocalize with experimental gliomas. Neurosurgery. 2007; 60:524–529. [PubMed: 17327798]
8. Kennedy BC, Maier LM, D'Amico R, Mandigo CE, Fontana EJ, Waziri A, Assanah MC, Canoll P, Anderson RC, Anderson DE, Bruce JN. Dynamics of central and peripheral immunomodulation in a murine glioma model. BMC Immunol. 2009; 10:11. [PubMed: 19226468]
9. VanHandel M, Alizadeh D, Zhang L, Kateb B, Bronikowski M, Manohara H, Badie B. Selective uptake of multi-walled carbon nanotubes by tumor macrophages in a murine glioma model. J Neuroimmunol. 2009; 208:3–39. [PubMed: 19181390]
10. Hoelzinger DB, Demuth T, Berens ME. Autocrine factors that sustain glioma invasion and paracrine biology in the brain microenvironment. J Natl Cancer Inst. 2007; 99:1583–1593. [PubMed: 17971532]
11. Hirschberg H, Baek S-K, Kwon YJ, Sun C-H, Madsen SJ. Bypassing the blood brain barrier: Delivery of therapeutic agents by macrophages. Proc SPIE. 2010; 7548:3Z-1-5.
12. Madsen SJ, Baek S-K, Makkouk AR, Krasieva T, Hirschberg H. Macrophages as cell-based delivery systems for nanoshells in photothermal therapy. Ann Biomed Eng. 2012; 40:507–515. [PubMed: 21979168]
13. Hirschberg H, Uzal FA, Chighvinadze D, Zhang MJ, Peng Q, Madsen SJ. Disruption of the blood–brain barrier following ALA-mediated photodynamic therapy. Lasers Surg Med. 2008; 40:535–542. [PubMed: 18798293]
14. Hirschberg H, Zhang MJ, Gach HM, Uzal FA, Peng Q, Sun C-H, Chighvinadze D, Madsen SJ. Targeted delivery of bleomycin to the brain using photo-chemical internalization of *Clostridium perfringens* epsilon prototoxin. J Neurooncol. 2009; 95:317–329. [PubMed: 19506813]
15. Mathews MS, Chighvinadze D, Gach HM, Uzal FA, Madsen SJ, Hirschberg H. Cerebral edema following photodynamic therapy using endogenous and exogenous photosensitizers in normal brain. Lasers Surg Med. 2011; 43:892–900. [PubMed: 22006731]
16. Wu J, Yang S, Luo H, Zeng L, Ye L, Lu Y. Quantitative evaluation of monocyte transmigration into the brain following chemical opening of the blood–brain barrier in mice. Brain Res. 2006; 1098:79–85. [PubMed: 16908012]
17. Maman N, Dhami S, Phillips D, Brault D. Kinetic and equilibrium studies of incorporation of di-sulfonated aluminum phthalocyanine into unilamellar vesicles. Biochim Biosphys Acta Biomebr. 1999; 1420:168–178.

18. Metz S, Bonaterra G, Rudelius M, Settles M, Rummeny EJ, Daldrup-Link HE. Capacity of human monocytes to phagocytose approved iron oxide contrast agents *in vitro*. Eur Radiol. 2004; 14:1851–1858. [PubMed: 15249981]
19. Oude Engberink RD, Blezer EL, Hoff EI, van der Pol SM, van der Toorn A, Dijkhuizen RM, de Vries HE. MRI of monocyte infiltration in an animal model of neuroinflammation using SPIO-labeled monocytes or free USPIO. J Cereb Blood Flow Metab. 2008; 28:841–851. [PubMed: 18000513]
20. Valable S, Barbier EL, Bernaudin M, Roussel S, Segebarth C, Petit E. Remy C *in vivo* MRI tracking of exogenous monocytes/ macrophages targeting brain tumors in a rat model of glioma. Neuroimage. 2008; 40:973–983. [PubMed: 18441552]
21. deBoer AG, Gaillard PJ. Drug targeting to the brain. Annu Rev Pharmacol Tocicol. 2007; 47:323–355.
22. Pardridge WM. Blood–brain barrier delivery. Drug Discov Today. 2007; 12:54–61. [PubMed: 17198973]
23. Thorek DL, Chen AK, Czupryna J, Tsourkas A. Super-paramagnetic iron oxide nanoparticle probes for molecular imaging. Ann Biomed Eng. 2006; 4:23–38. [PubMed: 16496086]
24. Weissleder R, Stark DD, Engelstad BL, Bacon BR, Compton CC, White DL, Jacobs P, Lewis J. Superparamagnetic iron oxide: Pharmacokinetics and toxicity. Am J Roentgenol. 1989; 152:167–173. [PubMed: 2783272]
25. Weinstein JS, Varallyay CG, Dosa E, Gahramanov S, Hamilton B, Rooney WD, Muldoon LL, Neuwelt EA. Super-paramagnetic iron oxide nanoparticles: Diagnostic magnetic resonance imaging and potential therapeutic applications in neurooncology and central nervous system inflammatory pathologies, a review. J Cereb Blood Flow Metab. 2010; 30:15–35. [PubMed: 19756021]
26. Madsen SJ, Sun C-H, Tromberg BJ, Hirschberg H. Development of a novel indwelling balloon applicator for optimizing light delivery in photodynamic therapy. Lasers Surg Med. 2001; 29:406–412. [PubMed: 11891728]
27. Angell-Petersen E, Hirschberg H, Madsen SJ. Determination of fluence rate and temperature distributions in the rat brain; implications for photodynamic therapy. J Biomed Opt. 2007; 12:0140031–9.
28. Madsen, SJ.; Wilson, BC. Optical properties of brain tissue. In: Madsen, SJ., editor. Optical methods and instrumentation in brain imaging and therapy. New York: Springer; 2013. p. 1-22.
29. Madsen SJ, Hirschberg H. Site-specific opening of the blood–brain barrier. J Biophoton. 2010; 3:356–367.
30. Kinoshita M, McDannold N, Jolesz FA, Hynynen K. Targeted delivery of antibodies through the blood–brain barrier by MRI-guided focused ultrasound. Biochem Biophys Res Commun. 2006; 340:1085–1090. [PubMed: 16403441]
31. Kinoshita M, McDannold N, Jolesz FA, Hynynen K. Noninvasive localized delivery of Herceptin to the mouse brain by MRI-guided focused ultrasound-induced blood–brain barrier disruption. Proc Natl Acad Sci USA. 2006; 103:11719–11723. [PubMed: 16868082]
32. Treat LH, McDannold N, Vykhodtseva N, Zhang Y, Tam K, Hynynen K. Targeted delivery of doxorubicin to the rat brain at therapeutic levels using MRI-guided focused ultrasound. Int J Cancer. 2007; 121:901–907. [PubMed: 17437269]
33. Etame AB, Diaz RJ, O'Reilly MA, Smith CA, Mainprize TG, Hynynen K, Rutka JT. Enhanced delivery of gold nano-particles with therapeutic potential into the brain using MRI-guided focused ultrasound. Nanomedicine. 2012; 8:1133–1142. [PubMed: 22349099]
34. Vykhodtseva N, McDannold N, Hynynen K. Progress and problems in the application of focused ultrasound for blood–brain barrier disruption. Ultrasonics. 2008; 48:279–296. [PubMed: 18511095]
35. Sporn LA, Foster TH. Photofrin and light induces microtubule depolymerization in cultured human endothelial cells. Cancer Res. 1992; 52:3443–3448. [PubMed: 1534512]
36. Fingar VH. Vascular effects of photodynamic therapy. J Clin Laser Med Surg. 1996; 14:323–328. [PubMed: 9612199]

37. Baek S-K, Makkouk AR, Krasieva T, Sun C-H, Madsen SJ, Hirschberg H. Photothermal treatment of glioma: An *in vitro* study of macrophage-mediated delivery of gold nanoshells. J Neurooncol. 2011; 104:439–448. [PubMed: 21221712]

38. Wilson BC, Patterson MS. The physics, biophysics and technology of photodynamic therapy. Phys Med Biol. 2008; 53:R61–R109. [PubMed: 18401068]

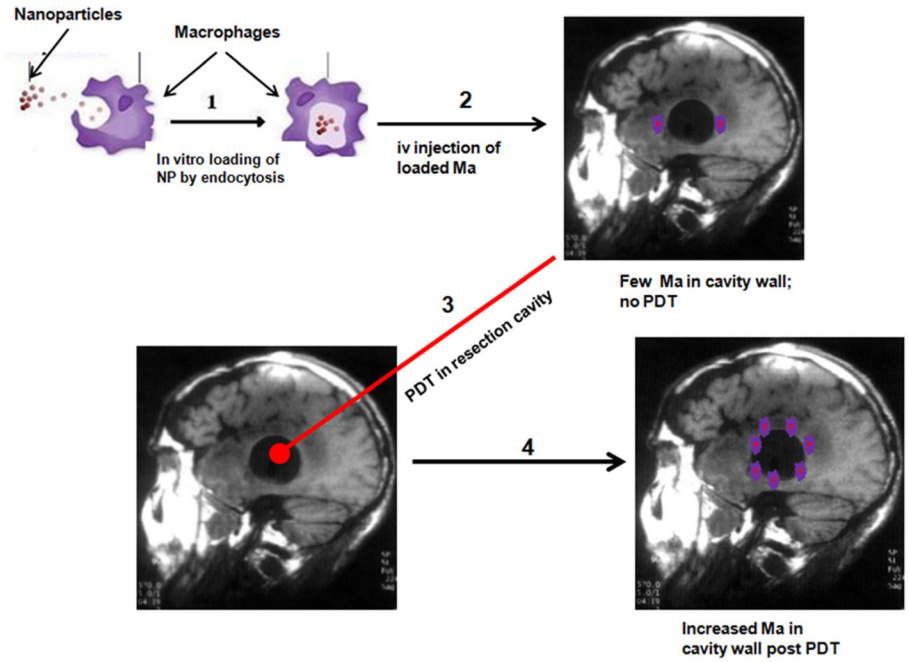

Fig. 1.

Basic concept of PDT-mediated macrophage delivery of nanoparticles in the postoperative resection cavity.

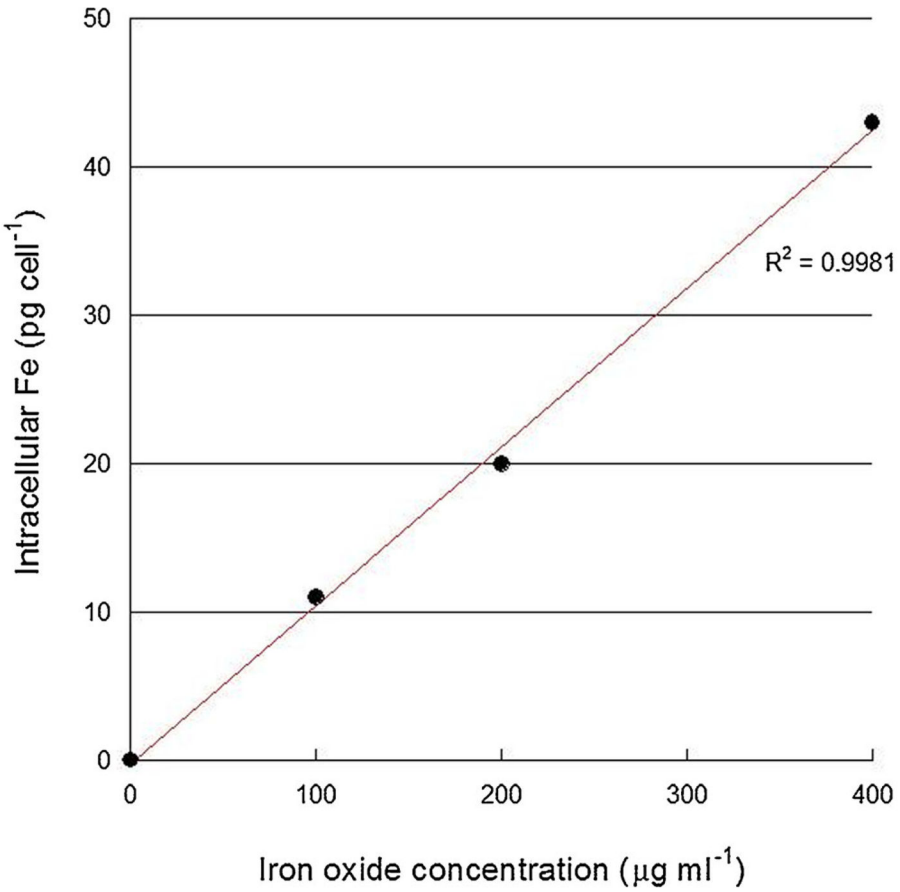

Fig. 2.

Iron oxide uptake in rat macrophages. Macrophages were incubated with Feridex® iron oxide nanoparticles for 24 hours and iron uptake was assessed by ICP-AES. Each point represents the mean of four experiments and error bars (within data points) denote standard deviations.

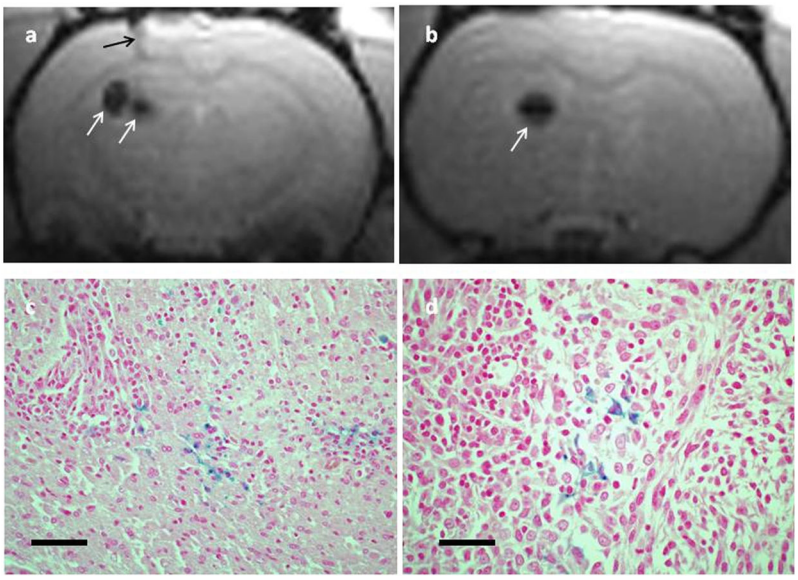

Fig. 3.

T_2^*-weighted axial MR images (**a**, **b**) showing signal voids (white arrows) in normal rat brain following intracranial injection of iron oxide-loaded macrophages. The black arrow in (a) denotes the injection track. The locations of the voids correspond to the point of Ma injection as determined from the coordinates on the stereotactic frame. Images were acquired 3 days postinjection. The images were acquired at two different levels (4 mm separation) in the same animal. Representative histological sections (**c**, **d**) from the same animal acquired 7 days post iron oxide-loaded macrophage administration. Sections were stained with both H&E and Perls. There is clear evidence of iron oxide (blue stain) thus confirming the MRI findings. The scale bars in (c) and (d) correspond to 80 and 40 μm, respectively.

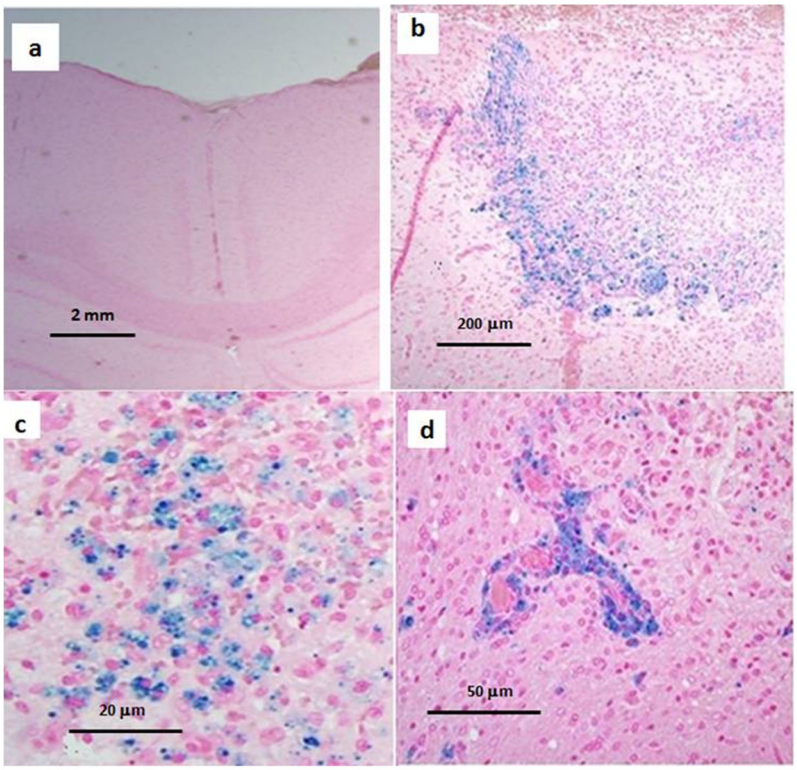

Fig. 4.

Representative sections of normal rat brain sectioned 7 days post-PDT. Iron oxide-loaded macrophages were administered immediately prior to PDT. Each section was stained with both H&E and Perls. No evidence of iron oxide following i.v. administration of 4.5×10^5 nanoparticle-loaded macrophages was observed in non-PDT controls (**a**). The presence of iron oxide is indicated by the blue around the periphery of the PDT-treated region (**b**). A combination of resident brain cells along with both endogenous and exogenous macrophages can be seen infiltrating the PDT-treated region in (**c**). Iron oxide-loaded macrophages are observed around capillary vessels in (**d**).

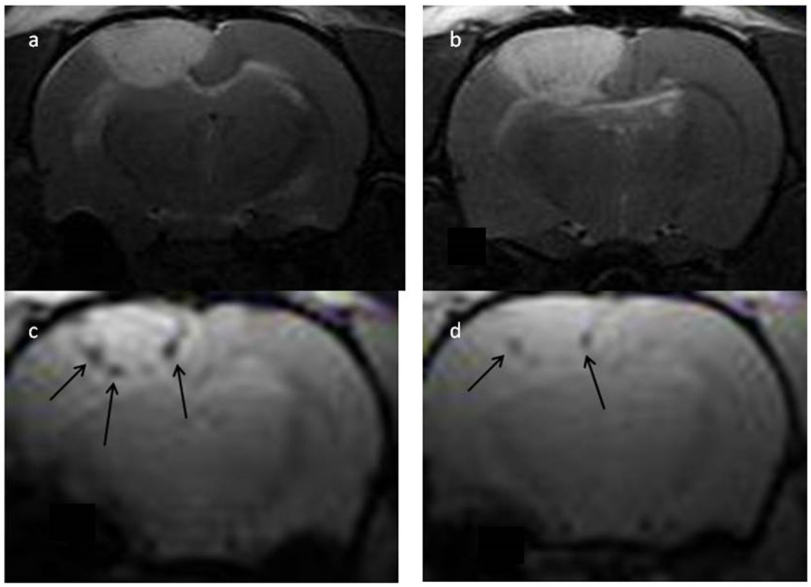

Fig. 5.

T_2- (**a**, **b**) and T_2^*-weighted (**c**, **d**) images of non-tumor rat brain acquired 24 hours post-PDT. Iron oxide-loaded macrophages were administered i.v. prior to PDT. The T_2 images show significant edema due to PDT-induced BBB breakdown. Signal voids (black arrows) are evident in the T_2^* images and are highly suggestive of the presence of iron oxide-loaded Ma. The distance from the surface of the brain to the distal edema boundary is approximately 4 mm.